International Journal of Fatigue 167 (2023) 107331

Contents lists available at ScienceDirect

International Journal of Fatigue

journal homepage: www.elsevier.com/locate/ijfatigue

Nanograin formation and cracking mechanism in Ti alloys under very high cycle fatigue loading

Chengqi Sun [a,b,*], Han Wu [a,b], Weiqian Chi [a,c], Wenjing Wang [c], Guang-Ping Zhang [d,*]

[a] State Key Laboratory of Nonlinear Mechanics, Institute of Mechanics, Chinese Academy of Sciences, Beijing 100190, China
[b] School of Engineering Science, University of Chinese Academy of Sciences, Beijing 100049, China
[c] Key Laboratory of Vehicle Advanced Manufacturing, Measuring and Control Technology (Beijing Jiaotong University), Ministry of Education, Beijing 100044, China
[d] Shenyang National Laboratory for Materials Science, Institute of Metal Research, Chinese Academy of Sciences, Shenyang 110016, China

ARTICLE INFO

Keywords:
Titanium alloy
Very high cycle fatigue
Twinning
Nanograins
Cracking mechanism

ABSTRACT

This paper shows that nanograins appear in a locally high-stress region for very high cycle fatigue of TC17 alloy, and twinning is a main contributor to nanograin formation. The locally high stress results in twinning or slip in preferentially oriented α grains. Then, the interaction between twin systems or dislocations induces the formation of dislocation cells or walls, nucleation of microbands, and finally the nanograins. As a result, the nanograin regions and the boundaries between the nanograin and coarse grain regions become preferential sites for crack initiation and early growth. The finite element analysis demonstrates the nanograin-related fatigue cracking behavior.

1. Introduction

Fatigue failure is a common phenomenon in metals under alternating loadings [1–6]. In recent decades, numerous results have shown that metallic materials could still fail at the stress lower than the traditional fatigue limit defined at 10^7 cycles [7–14]. The fatigue behavior exceeding 10^7 cycles (i.e., very high cycle fatigue, VHCF) has drawn great attention due to the high reliability and long-life requirements of some key parts in modern industry, e.g., aero-engine blades or high-speed strain axles often endure more than 10^8 even 10^{10} cyclic loadings in service.

Microstructure is an intrinsic and essential factor dominating the damage evolution under fatigue loadings and thus determines the failure mechanism to an extent. Differing from the low cycle and high cycle fatigue failure, the fracture surface in VHCF regime usually exhibits a fine granular area (FGA) (or rough area) feature in the crack initiation and early growth region, especially for titanium alloys and high-strength steels [7–12]. FGA is arguably the most significant feature in VHCF as it consumes almost all the fatigue life and the equivalent crack growth rate in FGA is much lower than 10^{-10} m/cycle [7,13–15]. This failure mechanism essentially distinguishes it from the traditional crack nucleation in grains, at grain boundaries or defects due to dislocation accumulation or slip band in metals [16,17]. The microstructure changes in FGA compared with the original material, and it could be a thin layer of nanograins [10,11,18,19] or discontinuous regions of nanograins [5,8,12–15,18,20].

Up till now, there are different viewpoints on the formation of nanograins in FGA under VHCF loading. One is that the nanograin formation in FGA is due to the dislocation interaction caused by the locally high strain during the cyclic loading [10,12,14,15,21]. The nanograins cause the crack initiation, and then the formed crack induces the further nanograin formation and crack formation, and finally the FGA forms. Another one is that the nanograins in FGA are the results of repeating contact of crack surfaces [18,19,22]. In this scenario, the nanograins form after the fatigue crack formation, implying that the nanograin formation is not related to the crack initiation and evolution. Evidently, such an argument may give rise to some basic questions. What is the mechanism of nanograin formation? How does it influence the crack initiation and early growth in VHCF regime? These pending questions still need to be clarified by direct evidence through experimental observations of the intermediate process of crack initiation and early growth that manifests the microstructure evolution during fatigue loadings.

In this paper, the direct experimental evidence is presented on the formation of nanograins to clarify the mechanism of crack initiation and damage evolution of Ti alloys in VHCF regime. At first, the fatigue test

* Corresponding authors.
E-mail addresses: scq@lnm.imech.ac.cn (C. Sun), gpzhang@imr.ac.cn (G.-P. Zhang).

https://doi.org/10.1016/j.ijfatigue.2022.107331
Received 21 June 2022; Received in revised form 9 October 2022; Accepted 10 October 2022
Available online 17 October 2022

was conducted on plate specimens of a TC17 titanium alloy by an ultrasonic frequency fatigue testing system. Then, the microstructure characteristic at the crack initiation and early growth region, the non-cracking region and the mated crack surfaces are characterized by scanning electron microscope (SEM), electron backscatter diffraction (EBSD) and transmission electron microscope (TEM). Finally, the basic mechanism of the nanograin formation and nanograin-induced fatigue cracking in VHCF regime is proposed based on the experimental observation and finite element analysis.

2. Materials and methods

2.1. Materials

The material used is a TC17 alloy, which is widely applied in aero-engines. The chemical composition is 4.97 Al, 4.19 Cr, 4.12 Mo, 2.09 Sn, 1.90 Zr, 0.11O, less than 0.10 Fe and balanced Ti in weight percent. It was at first under beta forging, then solid solution for 4 h at 800 °C and cooled by water, and finally under aging treatment for 8 h at 620 °C. All the specimens were cut from the solid bar after heat treatment. The tensile strength and yield strength are 1145 MPa and 1061 MPa, respectively. They were conducted on two cylindrical specimens with a gauge length of 30 mm and a diameter of 5 mm by a servo-hydraulic testing system.

2.2. Testing methods and characterization

The fatigue test was performed by an ultrasonic fatigue testing system USF-2000A with a frequency of 20 kHz in air and at room temperature. The resonant frequency was between 19.5 and 20.5 kHz for the testing specimen. It decreased with the increase of fatigue damage or crack growth. Once the resonant frequency was lower than 19.5 kHz, the fatigue test stopped. The fatigue loading was controlled by the displacement at specimen's ends, and it was at first transformed into the displacement by the theoretical formula [23]. The stress ratio was $R = -1$. The continuous fatigue loading was used, and compressive cold air was employed to cool the temperature of the specimen's smallest section during the fatigue test. The fatigue specimen is shown in Fig. 1. Before the fatigue test, the surface of the tested section of the specimen was ground and polished. The surface roughness R_a is less than 0.4 μm. The surface temperature of the specimens at the lowest tested stress amplitude $\sigma_a = 588$ MPa and the highest tested stress amplitude $\sigma_a = 651$ MPa was measured through a thermocouple (k-type) adhered to the surface of the smallest section by the polyimide tape during the fatigue test [15]. The stable temperature is about 39 °C at the stress amplitude of 588 MPa and 41 °C at the stress amplitude of 651 MPa.

The fatigue fracture surfaces were observed by SEM. By employing the focused ion beam (FIB) technique, micro cross-sectional samples were extracted in the crack initiation and early growth region, and then observed by EBSD and TEM to characterize the microstructure characteristic. The non-cracking region and mated crack surfaces were also observed by SEM and EBSD for a further examination of the microstructure evolution during the fatigue loading. The sample was at first cut from a fatigued specimen in VHCF regime, and ground by 1000 grit, 3000 grit, and 5000 grit abrasive papers with a water lubricant along the loading direction. Then, it was polished by 0.25 μm OP-S suspension, and finally polished for about 6 h using the VibroMet 2 vibratory polisher system with non-crystallizing colloidal silica polishing suspension.

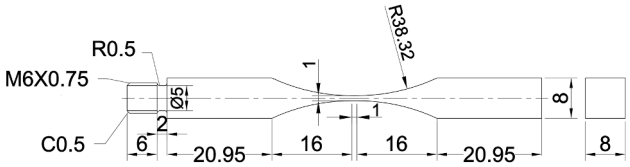

Fig. 1. Shape and dimension (in mm) of the fatigue specimen.

3. Experimental results and analyses

3.1. Microstructure

The microstructure is basketweave with lamellar α phase. EBSD results of the microstructure parallel to the loading direction are shown in Fig. 2. Fig. 2a and 2b are the inverse pole figure (IPF) and phase map of the microstructure, respectively. The enlarged view of the local microstructure is shown in Fig. 2c and 2d, respectively.

3.2. Stress-life data

The stress-life data of the tested specimens are shown in Fig. 3. It is seen that the present TC17 alloy could fail in VHCF regime, and the fatigue life has the tendency to increase with decreasing the stress amplitude.

3.3. Observation of nanograin formation during VHCF loading

SEM observation indicates that the failed specimens in Fig. 3 have an apparent main crack on the specimen surface with a width of 8 mm in the gauge section except for one failed specimen in VHCF regime with multiple micro cracks on the specimen surface, as shown in Fig. 4a. The rough area feature is also observed on the fracture surface of the specimen failed in VHCF regime (Fig. 4b and 4c), similar to that observed for the same TC17 alloy under conventional frequency fatigue test [8] and the Ti-6Al-4V alloy under ultrasonic frequency fatigue test [11].

To understand the microstructure evolution during the VHCF loading, two micro samples were at first extracted in the crack initiation and early growth region (i.e., the locations indicated by the short lines in Fig. 4c) along the loading direction through FIB technique and then their microstructures were characterized by EBSD and TEM. It is observed that there is a large lamellar α grain at the crack surface for sample 1 and some nanograins exist in the local region of this large α grain (Fig. 4e and 4f). The nanograins can still be visible for sample 2 shown in Fig. 4i and 4j although the IPF and phase map are not very clear for the grains quite close to the fracture surface. These nanograins are further identified in regions I and II by TEM observation, as shown in Fig. 4l. The selected area diffraction (SAD) patterns are composed of a series of diffused rings, indicating the existence of many nanograins with random orientation. The nanograins in α grains are not found in the original material without suffering from fatigue loading (Fig. 2). These results demonstrate that the nanograins form during the fatigue process. Moreover, a micro crack is observed below the crack surface from the SEM observation (Fig. 4h). It forms within the coarse α grain, coarse β grain, at α nanograin boundaries and the boundaries between α nanograin and coarse β grain from the IPF and phase map in Fig. 4i and 4j. The micro slip bands in α grains are also observed a little far from the crack surface (Fig. 4l and 4m).

3.4. Nanograins at non-cracking region and mated crack surfaces

To further understand the relationship between nanograin formation and crack initiation, the microstructure is examined for a specimen experiencing VHCF loading of 1.37×10^8 cycles under the stress amplitude $\sigma_a = 588$ MPa. This specimen has no main crack but multiple micro cracks on the specimen surface. It is found that some nanograins have formed in the non-cracking region. Fig. 5a shows the SEM image of a non-cracking region of the fatigued specimen. The nanograins in the non-cracking region are identified by the IPF and phase map in Fig. 5b and 5c. Moreover, the nanograins appear at the micro crack tip in the specimen after VHCF loading, as shown in Fig. 5i-5k and 5u-5w. Fig. 5i-5k are the SEM image, IPF and phase map of the micro crack tip in region

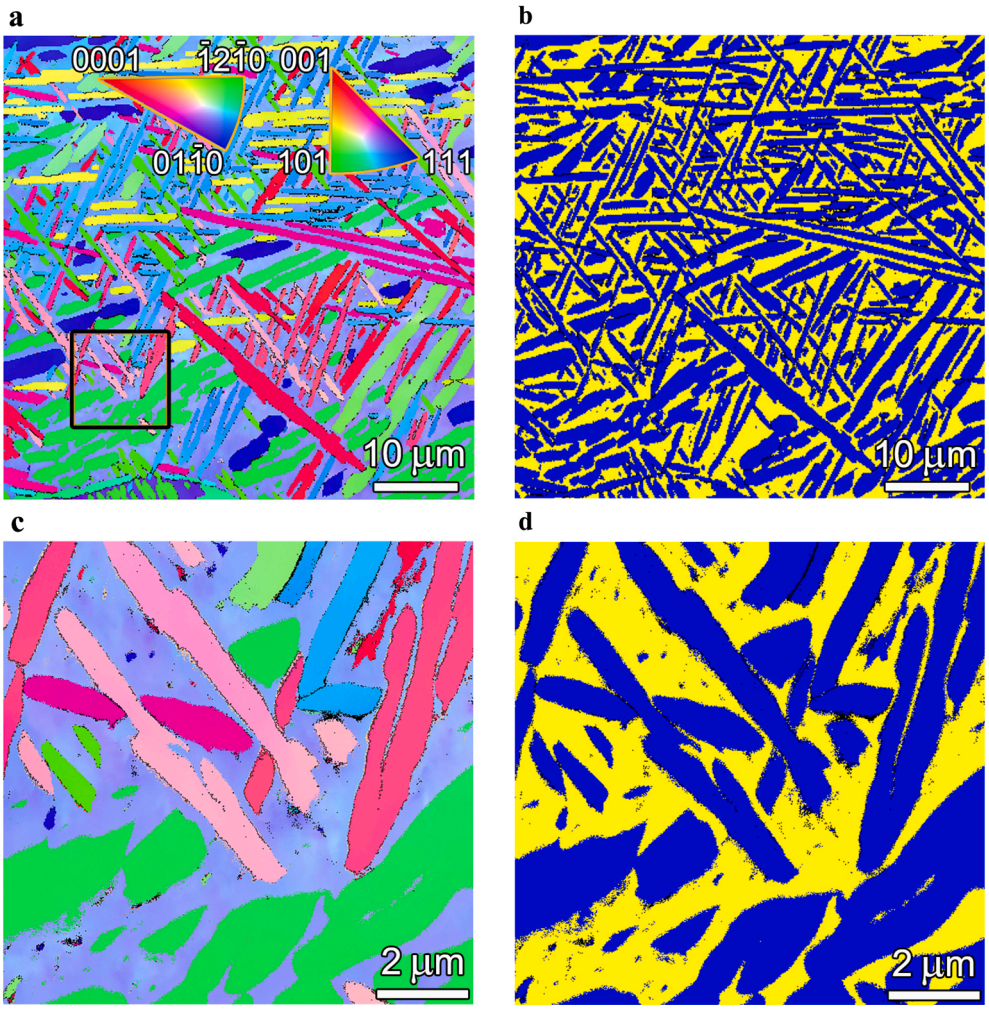

Fig. 2. Microstructure of the TC17 alloy. a and b: IPF and phase map (blue color: α phase, yellow color: β phase). c and d: close-ups of IPF and phase map for the rectangular region in a, respectively. (For interpretation of the references to color in this figure legend, the reader is referred to the web version of this article.)

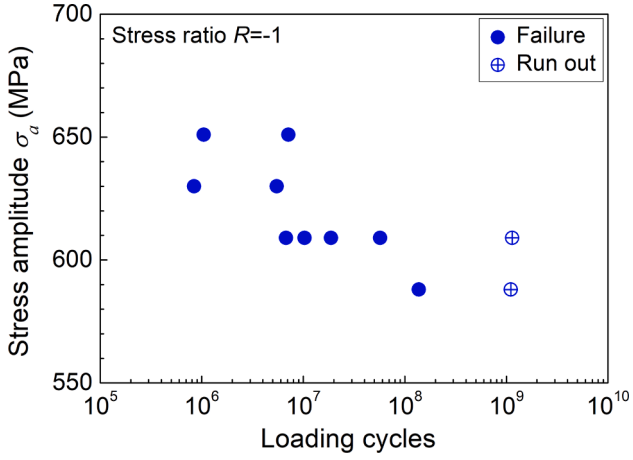

Fig. 3. Stress-life data of tested specimens.

1 in Fig. 5e, respectively, and Fig. 5u-5w are the SEM image, IPF and phase map of the micro crack tip in region 4 in Fig. 5e, respectively. This indicates that the nanograin formation is not only the result of the high stress at crack tip. It can happen before the formation of micro cracks during the VHCF loading. Then, the micro cracks could nucleate along the boundaries between the nanograin and the coarse grain or within the nanograin regions due to the microstructural inhomogeneity caused by nanograins, as shown in Fig. 5m-5o and 5q-5s. Fig. 5m-5o are the SEM image, IPF and phase map of the micro crack in region 2 in Fig. 5e, respectively, and Fig. 5q-5s are the SEM image, IPF and phase map of the micro crack in region 3 in Fig. 5e, respectively.

4. Discussion

4.1. Deformation twins and nanograin formation mechanism

The findings in *Sec*. 3.4 clearly provide a clue for the micro crack formation, which is related to the formation of α nanograins. This stimulates us to find the basic mechanism of how the α nanograins generate under VHCF loading. Then, some α grains (hexagonal close-packed structure) are carefully examined for the present TC17 alloy after VHCF loading, and deformation twins are found in the non-cracking region by the analysis of EBSD data via HKL CHANNEL5 software. The deformation twins are identified through the grain boundaries satisfying the twin mode [24], and a tolerance of ± 5° deviation is used [25,26]. The Schmid factors for the parent grains and twin variants in the non-cracking region in Fig. 5b are shown in Fig. 6a. Extensive twins have also been observed at or very near the fatigue fracture surface in the crack initiation and early growth region in Fig. 5n, Fig. 4e and Fig. 4i. The corresponding Schmid factors for the parent grains and twin variants are shown in Fig. 6b-6d, respectively. This implies that the nanograin formation is associated with twinning behavior. The twinning

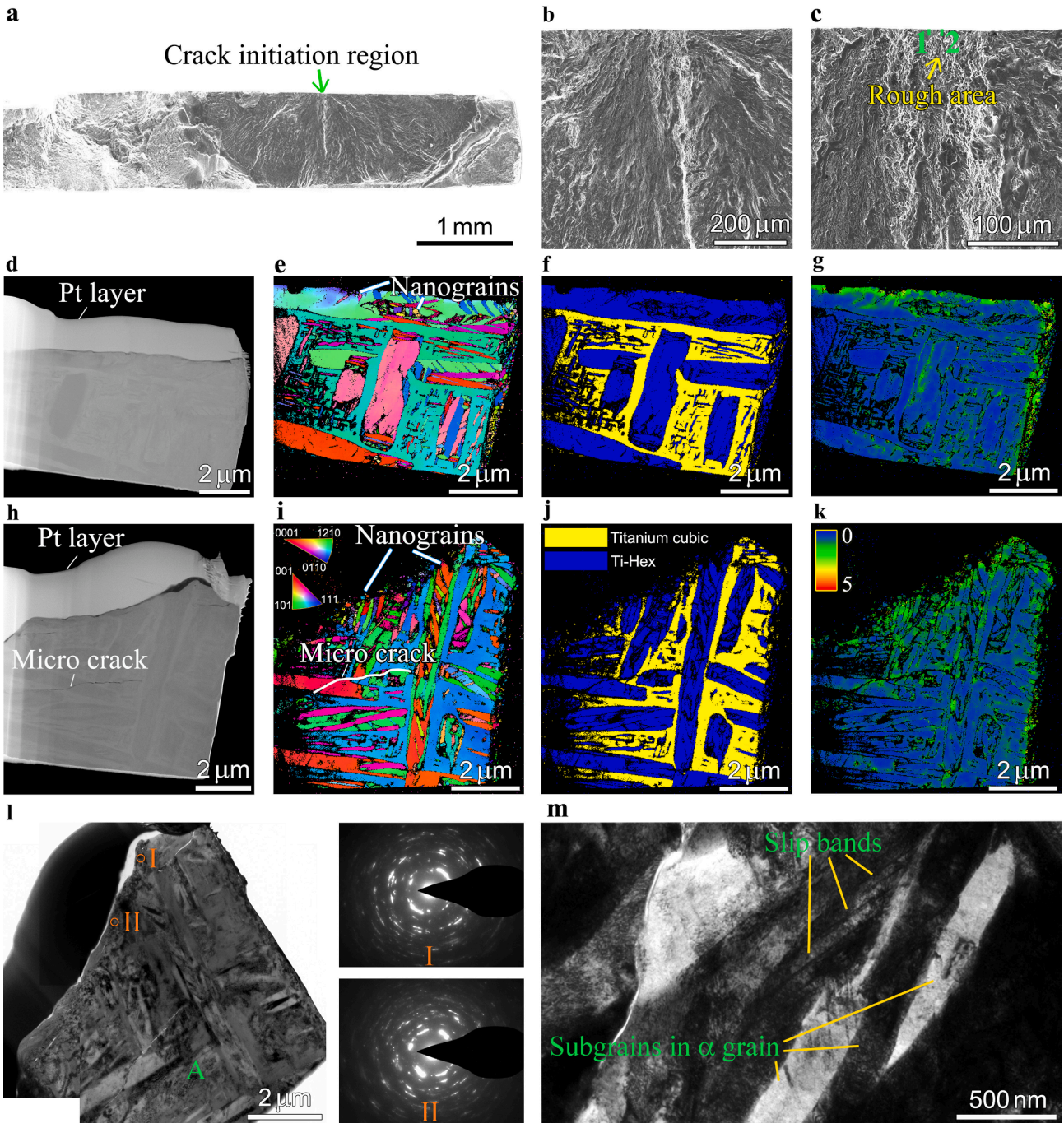

Fig. 4. SEM, EBSD and TEM observations of the specimen failed at 1.88×10^7 cycles under $\sigma_a = 609$ MPa. a: SEM image of the whole fracture surface. b and c: close-ups of the crack initiation and early growth region in a, the short lines in c denote the locations of extracted micro samples 1 and 2. d-g: SEM image, IPF, phase map and kernel average misorientation (KAM) map of extracted sample 1 in c, respectively. h-k: SEM image, IPF, phase map and KAM map of extracted sample 2 in c, respectively. l: TEM bright field image of extracted sample 2 in c, the SAD patterns are for the circular regions I and II just beneath the cracking surface, respectively. m: close-up of region A in l.

planes are $\{10\bar{1}1\}$ (compression twin) and $\{10\bar{1}2\}$ (extension twin). It is discovered that most of the Schmid factors for basal slip system are very small for the parent grains with $\{10\bar{1}1\}$ twins (Fig. 6). The associated Schmid factors for basal slip system of $\{10\bar{1}1\}$ twin variants are commonly increased compared to the parent grains, i.e., compression twins preferentially orient for basal slip. While for $\{10\bar{1}2\}$ twins, most of the Schmid factors for basal slip system of the parent grains are bigger, and the Schmid factors for basal slip system of $\{10\bar{1}2\}$ twin variants are generally decreased compared to the parent grains. These results indicate that the type of twinning system triggered during the fatigue loading depends on the initial orientation of grains and the deformation condition [27,28]. The values of KAM map in Fig. 4g and 4k, Fig. 5d and 5p further indicate that the deformation is often severe in the local region of the parent grain where the $\{10\bar{1}2\}$ twin forms. The dislocation tends to accumulate in the α grain with a bigger Schmid factor for basal slip system due to the locally high stress. When the dislocation accumulation reaches a value, twinning is triggered to meet the strain compatibility requirement. This could explain the reason why the $\{10\bar{1}2\}$ twin tends to appear in the parent grain with a bigger Schmid factor for basal slip system. Moreover, the secondary twinning is

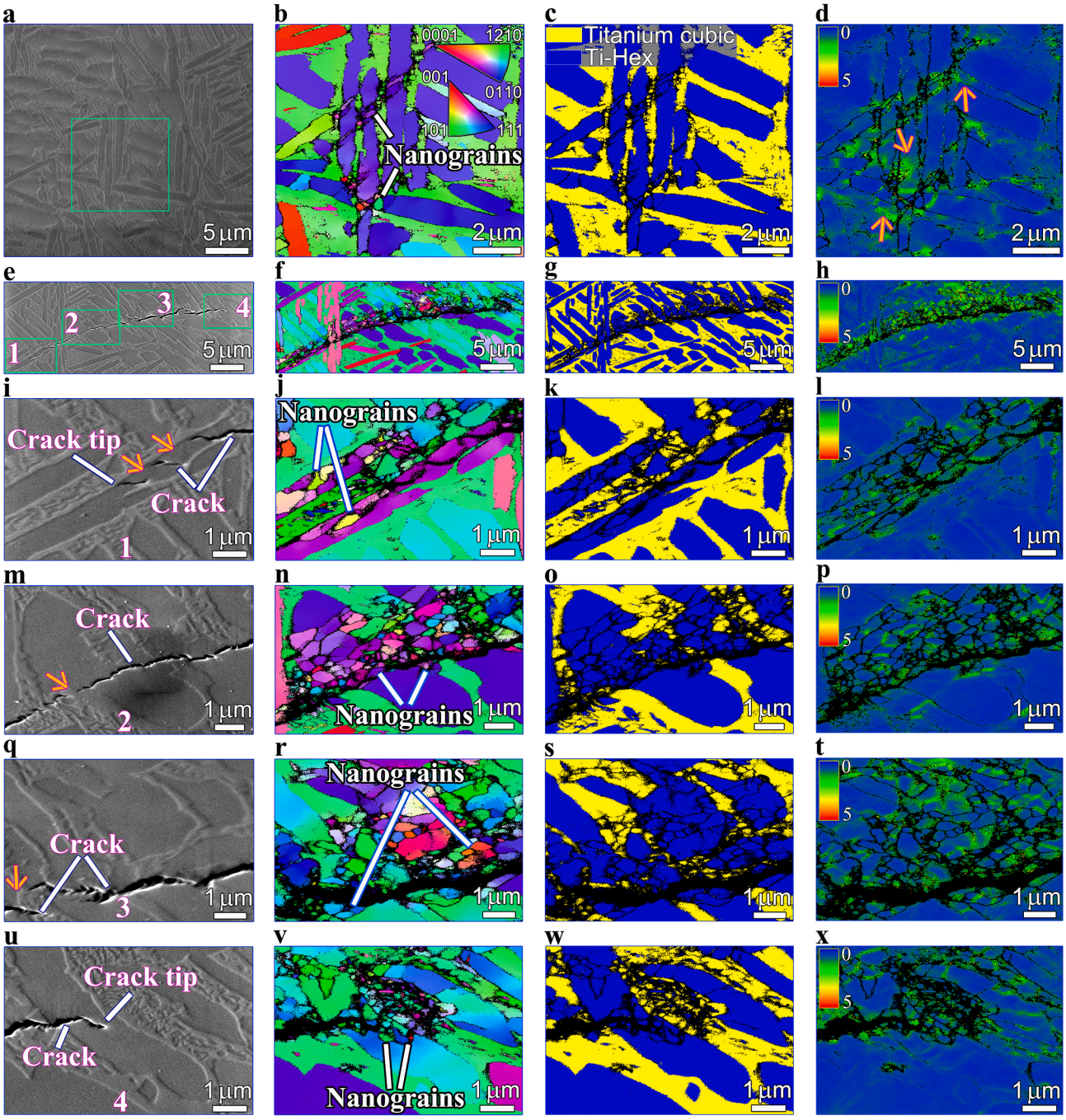

Fig. 5. SEM and EBSD observations for non-cracking region and mated crack surfaces of a fatigued specimen experiencing 1.37×10^8 cycles under $\sigma_a = 588$ MPa. a: SEM image of non-cracking region. b-d: IPF, phase map and KAM map corresponding to the rectangular region in a; arrows in d point to the bigger plastic strain regions. e: SEM image of a small crack. f-h: IPF, phase map and KAM map corresponding to e, respectively. i-l, m-p, q-t and u-x: close-ups of SEM image, IPF, phase map and KAM map of the rectangular regions 1–4 in e, respectively; arrows in i, m and q point to the unconnected region between micro cracks. Loading direction is up and down along the paper.

observed for the $\{10\bar{1}1\}$ twin variant (grain 2 in Fig. 6c). This suggests that the locally high-stress concentration caused by slip or twin interaction with grain boundaries could lead to further twinning during the fatigue loading.

Twinning is initiated by heterogeneous nucleation based on the results of single crystals of hexagonal close-packed metals, cadmium and zinc [29]. The dissociation of some dislocation configuration into a single-layered or multi-layered stacking fault leads to the twin nucleus. Under VHCF loading, the stress is lower and the plastic deformation only occurs in some local grains. The dislocations due to the locally high stress pile up during the fatigue loading and then the high-stress concentration results in twinning in preferentially oriented α grains [30,31]. The locally high stress during the further cyclic loading causes the twin growth by the steps of heterogeneous nucleation due to some extended defect configuration, the pole mechanism, cross-slip sources, etc. [29,32,33]. It is noted that twinning prevails at low temperatures and the higher frequency is favorable for twinning [29]. An analysis is also performed for the α grains in the crack initiation and early growth region (Fig. 6 in Ref. [8]) for the same TC17 alloy under the conventional frequency of 50 Hz in VHCF regime and the twinning phenomenon is

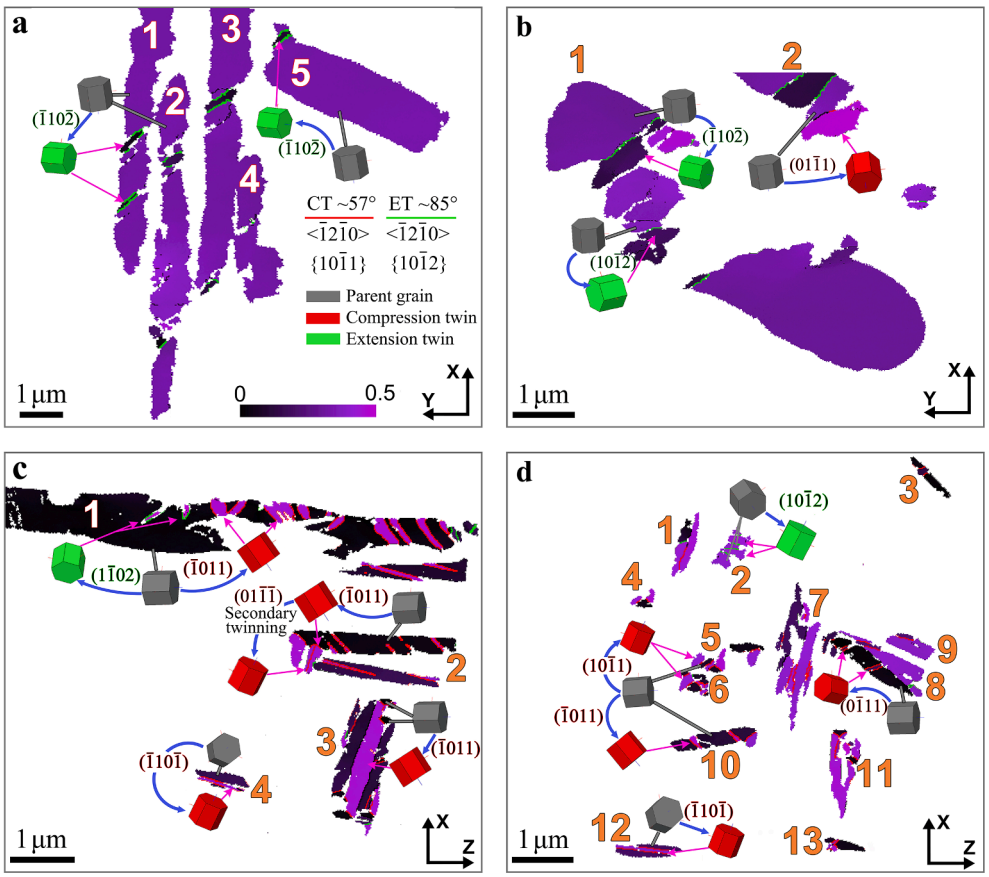

Fig. 6. Schmid factor for basal slip system. a-d: Parent grains and twin variants in Fig. 5b, Fig. 5n, Fig. 4e and Fig. 4i, respectively.

observed (Fig. 7). This result indicates that the formation of deformation twins in Ti alloys is a common phenomenon during the VHCF loading, which is independent of the loading frequency and loading type.

TC17 is an α + β titanium alloy. The β phase is a body-centered cubic structure and favors deformation, while the hexagonal close-packed α phase is relatively hard to deform. During the cyclic loading, the

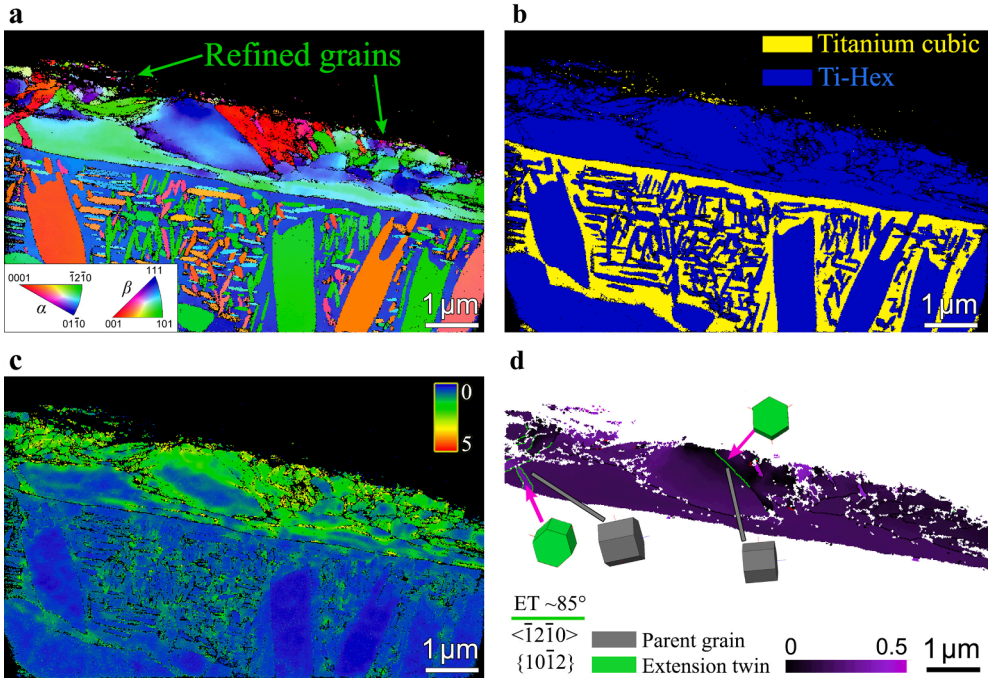

Fig. 7. EBSD results for the extracted sample in Fig. 6 in Ref. [8]. a-c: IPF, phase map and KAM map, respectively. d: Schmid factors for basal slip system of the parent grain and twin variants in a.

microstructural inhomogeneity and deformation incompatibility induce the locally high nonuniform deformation (e.g., the regions where the arrows point to in Fig. 5d) and the high-stress concentration leads to the occurrence of twinning in favorable α grains [30,31]. The interaction between twinning systems causes the formation of dislocation cells or walls, the nucleation of microbands, and then the formation of low angle and polygonal submicron grains, and further the nanograins [34]. The lamellar subgrains could also be caused by the crystallographical slip and the followed propagation by multiple or cross slips due to stress concentration [35]. The intersection of subboundaries further results in the smaller refined grains, and finally the nanograins. The slip bands and subgrains are both observed in the α grains for the present Ti alloy in VHCF regime (Fig. 4l and 4m). This indicates that the slip is also a contributor to the nanograin formation of Ti alloys [35,36]. The locally high stress causes this process during the cyclic loading. The rotation recrystallization might play an important role in the nanograin formation of Ti alloys during fatigue loading [35], which absorbs dislocations and accommodates further deformation [37].

4.2. VHCF cracking mechanism

The results in Figs. 4 and 5 indicate that fatigue cracks could initiate at the boundaries between nanograin and coarse grain regions or within nanograin regions, which reveals that the nanograins formed during the cyclic loading play a vital role in the crack initiation and early growth in VHCF regime. The nanograin formation increases the microstructural inhomogeneity in local regions, which promotes the crack initiation and early growth [38,39].

For a further validation, the finite element analysis on the stress field is performed for a region of coarse grains with local nanograins before crack formation by Abaqus software. The simulated region is created referring to the SEM image, IPF and phase map shown in Fig. 8a-8c, respectively. The geometric model with the boundary conditions and the loading direction is shown in Fig. 8d, and the thickness is 0.2 μm. The grains are regarded as anisotropic materials. The crystallographic orientation information is extracted from IPF by EBSD. The merged nodes are used to deal with the boundaries of different phases or grains, i.e., the nodes on the common edge are shared by adjacent phases or

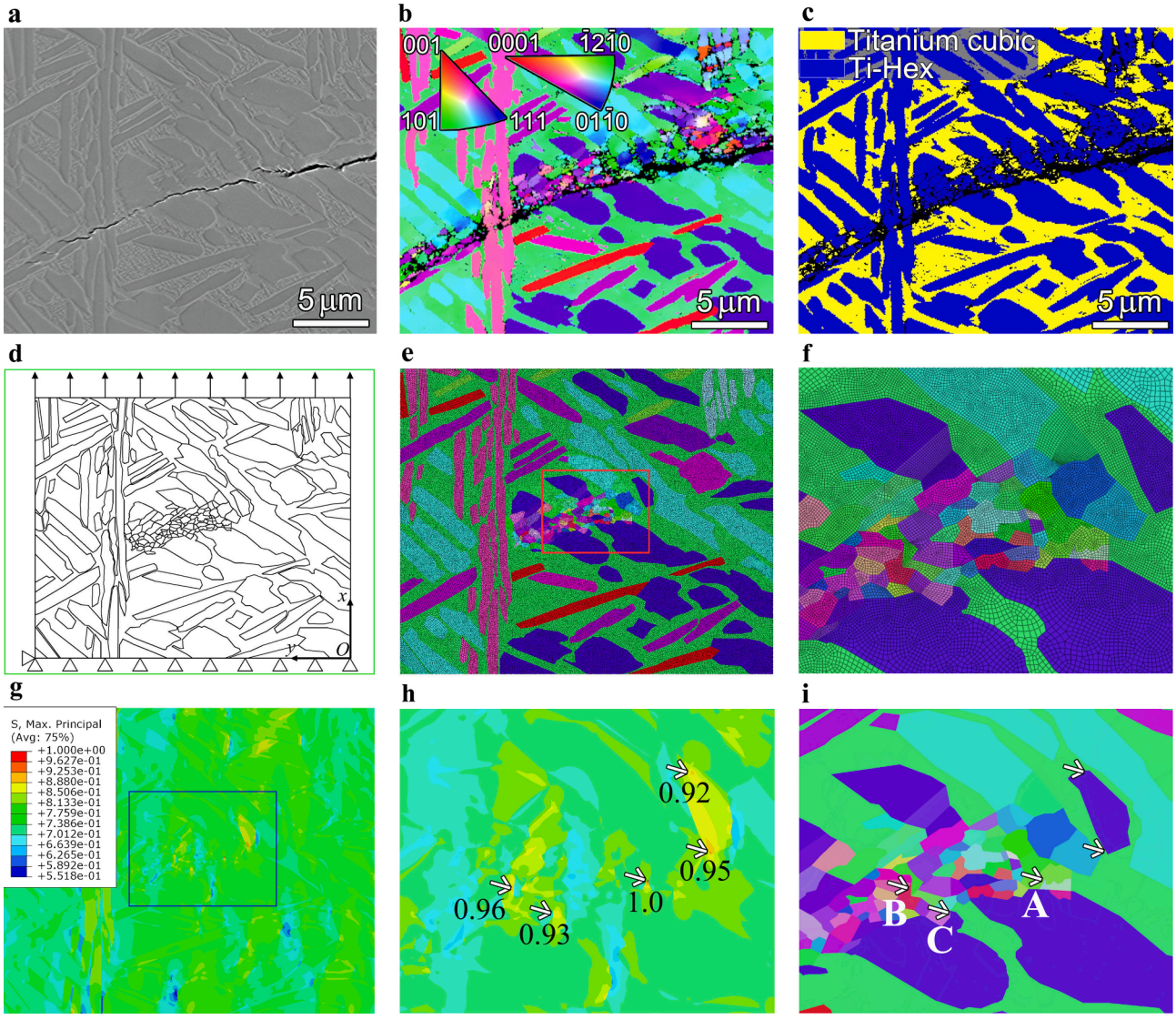

Fig. 8. Finite element analysis of a region with local nanograins. a-c: SEM image, IPF and phase map referred for the simulated region, respectively. d: geometric model with boundary conditions and loading direction by arrows, the thickness is 0.2 μm. e: meshes of the model, the colors denote the different crystallographic orientation. f: close-up of the rectangular region in e. g: first principal stress contour. h: close-up of the rectangular region in g, the arrows point to the location of the 5 dimensionless maximum stresses and the numbers indicate the values. i: the corresponding geometric model for h, the colors denote the different crystallographic orientation and the arrows point to the location of the 5 dimensionless maximum stresses.

grains. The single-crystal elastic constants of α and β phases are obtained from literature [40,41]. The finite element model is meshed by C3D8R (three-dimensional 8-noded hexahedral elements with reduced integration). The element size is 0.05 μm for the refined grain regions and 0.1 μm for the others, as shown in Fig. 8e and 8f, respectively. The results indicate that the stress could be quite high within nanograin regions (locations A and B in Fig. 8i) or along the boundary between the nanograin and coarse grain regions (location C in Fig. 8i) in the local region. It accords with the observation of crack path manifesting the nanograins in Fig. 5n and 5r in VHCF regime. The results for the crack initiation preferred within nanograin regions are also consistent with the experimental data that the stress-life curves merge in VHCF regime for the ultrafine-grained titanium and the coarse titanium [39]. Once the crack forms, it could grow along the boundaries between the nanograin and coarse grain regions or within nanograin regions due to the lower near-threshold crack growth resistance in refined grains [42,43]. The occurrence or growth of the crack increases the locally high stress at the crack tip and induces the further nanograin formation and crack extension under fatigue loadings.

On the other hand, the micro crack could nucleate at first in larger α-phase, α-phase clusters, α-β interfaces, etc. due to the microstructural inhomogeneity and deformation incompatibility in VHCF regime [44,45], namely that the micro crack formation could not need to undergo the process of nanograin formation. In this case, the nanograin formation is not a precursor to the crack initiation in VHCF regime. This is observed for the present Ti alloy (Fig. 5i-5k). In this case, the local nanograin formation (e.g., in the vicinity of a crack tip) might also occur due to the locally high stress at the crack tip during the following fatigue loading, similar to the nanograins formed at the crack tip in Fig. 5j and 5v.

Summarizing the above observations, the basic mechanism for the crack initiation and early growth of Ti alloys in VHCF regime is proposed below (Fig. 9): (i) The locally high stress due to dislocation accumulation causes the formation of twinning, slip or micro crack during the fatigue loading, as shown in Fig. 9(i). (ii) The interaction between twinning systems or dislocations induces the formation of dislocation cell or wall, further the microbands or submicron grains, and finally the nanograins. Then, the micro crack forms along the boundaries between the nanograin and coarse grain regions or within nanograins. Meanwhile, the micro crack could form in local regions due to the microstructure inhomogeneity and deformation incompatibility (i.e., irrespective of the nanograin formation) during this process, as shown in Fig. 9(ii). (iii) The locally high stress at the tip of crack (no matter it forms due to the nanograin formation or irrespective of the nanograin formation) promotes the formation of nanograins, and the nanograins again promote the micro crack growth. The micro crack grows or coalesces, and the growing crack causes the nanograin formation or micro crack formation again during the further fatigue loading, as illustrated in Fig. 9(iii); (iv) The process (iii) continues until the crack initiation and early growth stage is finished, as depicted in Fig. 9(iv).

Our model elucidates the process of crack initiation and early growth that manifests the microstructure evolution, and it for the first time incorporates the role of twinning in the nanograin formation and the followed cracks in Ti alloys during the VHCF loading. In comparison, the previous model on repeating contact of crack surfaces [11,19,22,46] cannot give a complete explanation for the nanograin formation in non-cracking regions and at crack tips, and the crack paths along the boundaries between the nanograin and coarse grain regions. In the scenario due to dislocation interaction, the deformation twins formed during the fatigue process are not observed and the role of twinning is

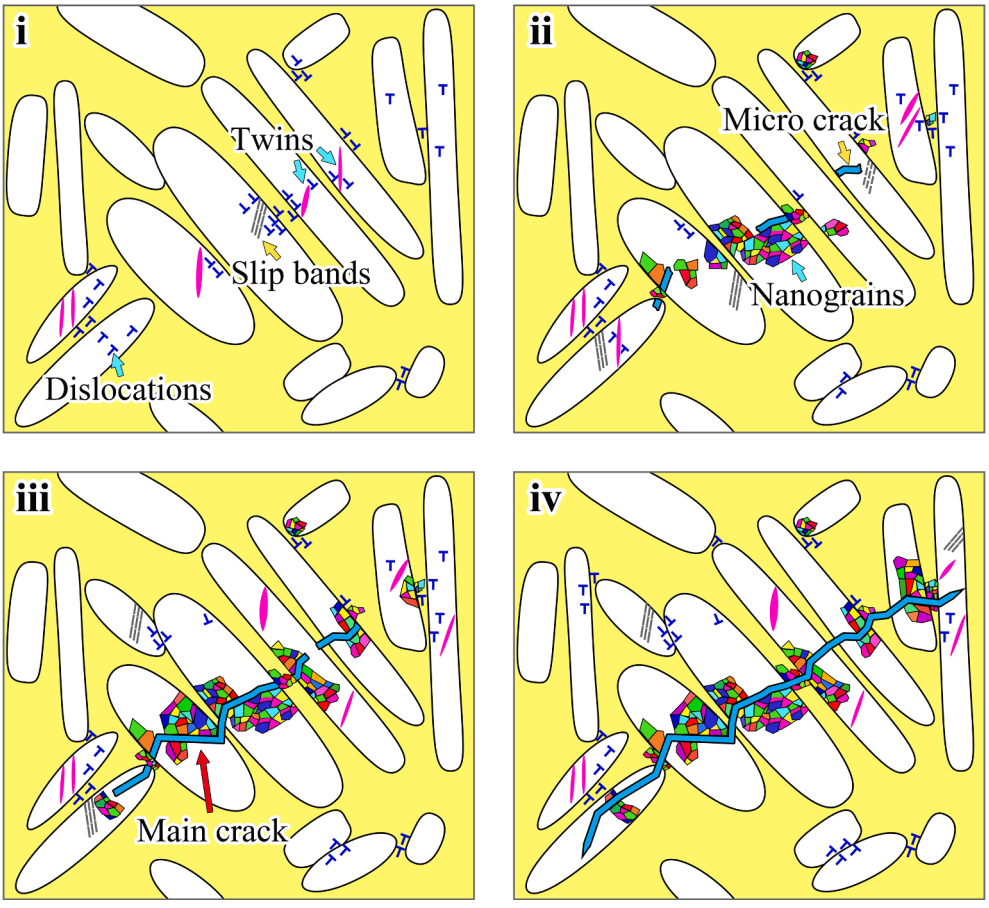

Fig. 9. Schematic of crack initiation and early growth of Ti alloys in VHCF regime.

not involved in the crack initiation and early growth accompanying with the microstructure evolution for Ti alloys [12,15]. The new model could explain the different microstructure characteristics (i.e., nanograin layers, local regions of nanograins, and no nanograin phenomenon) observed in the rough area for Ti alloys in VHCF regime [8,11,12,46]. It also explains the internal cracking from defects with a layer of nanograins in the rough area for VHCF of additively manufactured Ti alloys [47], namely that the stress concentration caused by the defect promotes the tendency of dislocation accumulation or twinning formation, and further the nanograin formation and micro cracks within nanograins, and finally the rough area with nanograin layer microstructure.

5. Conclusions

In this paper, the nanograin formation and cracking mechanism in VHCF regime are investigated for a TC17 alloy based on SEM, EBSD and TEM observations of the samples extracted in the crack initiation and early growth region and the sample cut from the fatigued specimen after VHCF loading. The main results are as follows:

(1) Deformation twins are found in the non-cracking region and at or very near the fatigue fracture surface in the crack initiation and early growth region under VHCF loading. For $\{10\bar{1}1\}$ twins, most of the Schmid factors for basal slip system of the parent grains are very small, and the Schmid factors for basal slip system of the $\{10\bar{1}1\}$ twin variants are commonly increased compared to the parent grains. While for $\{10\bar{1}2\}$ twins, most of the Schmid factors for basal slip system of the parent grains are bigger, and the Schmid factors for basal slip system of the $\{10\bar{1}2\}$ twin variants are generally decreased compared to the parent grains. The secondary twinning is observed for the $\{10\bar{1}1\}$ twin variant, indicating that the locally high-stress concentration caused by slip or twin interaction with grain boundaries could lead to further twinning during the fatigue loading.
(2) Nanograin formation is observed in α grains of the TC17 alloy after VHCF loading, and twinning is revealed to be a main contributor to the nanograin formation. The locally high-stress concentration results in the twinning or slip in preferentially oriented α grains. Then, the interaction between twin systems or dislocations induces the formation of dislocation cells or walls, the nucleation of microbands, and finally the nanograins.
(3) The nanograins formed during the fatigue process increase the microstructural inhomogeneity in local regions. As a result, the nanograin regions and the boundaries between the nanograin and coarse grain regions become preferential sites for crack initiation and early growth in VHCF regime. The finite element analysis demonstrates the nanograin-related fatigue cracking behavior. The crack initiation and early growth of Ti alloys in VHCF are attributed to the cracks caused by the nanograin formation due to twinning or dislocation sliding in combination with the cracks formed irrespective of the nanograin formation during the fatigue loading.

The findings advance a new insight into the failure mechanism of metals in fatigue, and may provide a guidance for the design of alloys with high resistance to VHCF.

Declaration of Competing Interest

The authors declare that they have no known competing financial interests or personal relationships that could have appeared to influence the work reported in this paper.

Data availability

Data will be made available on request.

Acknowledgements

The authors acknowledge the National Natural Science Foundation of China Basic Science Center for “Multiscale Problems in Nonlinear Mechanics” (11988102) and the National Natural Science Foundation of China (91860112).

References

[1] Suresh S, editor. Fatigue of Materials. Cambridge University Press; 1998.
[2] Pan Q, Zhou H, Lu Q, Gao H, Lu L. History-independent cyclic response of nanotwinned metals. Nature 2017;551(7679):214–7.
[3] Koyama M, Zhang Z, Wang M, Ponge D, Raabe D, Tsuzaki K, et al. Bone-like crack resistance in hierarchical metastable nanolaminate steels. Science 2017;355(6329):1055–7.
[4] Chandran KSR. Duality of fatigue failures of materials caused by Poisson defect statistics of competing failure modes. Nature Mater 2005;4(4):303–8.
[5] Li G, Sun C. High-temperature failure mechanism and defect sensitivity of TC17 titanium alloy in high cycle fatigue. J Mater Sci Technol 2022;122:128–40.
[6] Li L, Zhang Z, Zhang P, Wang Z, Zhang Z. Controllable fatigue cracking mechanisms of copper bicrystals with a coherent twin boundary. Nat Commun 2014;5:3536.
[7] Hong Y, Sun C. The nature and the mechanism of crack initiation and early growth for very-high-cycle fatigue of metallic materials – An overview. Theor Appl Fract Mech 2017;92:331–50.
[8] Chi W, Wang W, Xu W, Li G, Chen X, Sun C. Effects of defects on fatigue behavior of TC17 titanium alloy for compressor blades: Crack initiation and modeling of fatigue strength. Eng Fract Mech 2022;259:108136.
[9] Cervellon A, Hémery S, Kürnsteiner P, Gaultb B, Kontis P, Cormier J. Crack initiation mechanisms during very high cycle fatigue of Ni-based single crystal superalloys at high temperature. Acta Mater 2020;188:131–44.
[10] Grad P, Reuscher B, Brodyanski A, Kopnarski M, Kerscher.. E Mechanism of fatigue crack initiation and propagation in the very high cycle fatigue regime of high-strength steels. Scr Mater 2012;67:838–41.
[11] Su H, Liu X, Sun C, Hong Y. Nanograin layer formation at crack initiation region for very-high-cycle fatigue of a Ti–6Al–4V alloy. Fatigue Fract Eng Mater Struct 2017;40(6):979–93.
[12] Sun C, Chi W, Wang W, Duan Y. Characteristic and mechanism of crack initiation and early growth of an additively manufactured Ti-6Al-4V in very high cycle fatigue regime. Int J Mech Sci 2021;205:106591.
[13] Sun C, Song Q, Zhou L, Liu J, Wang Y, Wu X, et al. The formation of discontinuous gradient regimes during crack initiation in high strength steels under very high cycle fatigue. Int J Fatigue 2019;124:483–92.
[14] Song Q, Sun.. C Mechanism of crack initiation and early growth of high strength steels in very high cycle fatigue regime. Mater Sci Eng A 2020;771:138648.
[15] Chi W, Li G, Wang W, Sun C. Interior initiation and early growth of very high cycle fatigue crack in an additively manufactured Ti-alloy. Int J Fatigue 2022;160:106862.
[16] Tanaka K, Mura T. A dislocation model for fatigue crack initiation. Int J Appl Mech 1981;48(1):97–103.
[17] Lavenstein S, Gu Y, Madisetti D, El-Awady J. The heterogeneity of persistent slip band nucleation and evolution in metals at the micrometer scale. Science 2020;370:eabb2690.
[18] Ritz F, Stäcker C, Beck T, Sander M. FGA formation mechanism for X10CrNiMoV12-2-2 and 34CrNiMo6 for constant and variable amplitude tests under the influence of applied mean loads. Fatigue Fract Eng Mater Struct 2018;41(7):1576–87.
[19] Hong Y, Liu X, Lei Z, Sun C. The formation mechanism of characteristic region at crack initiation for very-high-cycle fatigue of high-strength steels. Int J Fatigue 2016;89:108–18.
[20] Gao G, Liu R, Fan Y, Qian G, Gui X, Misra RDK, et al. Mechanism of subsurface microstructural fatigue crack initiation during high and very-high cycle fatigue of advanced bainitic steels. J Mater Sci Technol 2022;108:142–57.
[21] Zhang H-J, Yu F, Li S-X, He E-G. Fine granular area formation by damage-induced shear strain localization in very-high-cycle fatigue. Fatigue Fract Eng Mater Struct 2021;44(9):2489–502.
[22] Nakamura T, Oguma H, Shinohara Y. The effect of vacuum-like environment inside sub-surface fatigue crack on the formation of ODA fracture surface in high strength steel. Procedia Eng 2010;2(1):2121–9.
[23] Bathias C, Paris P. Gigacycle fatigue in mechanical practice. CRC Press; 2004.
[24] Crawforth P. Towards a micromechanistic understanding of imparted subsurface deformation during machining of titanium alloys. Sheffield Univ; 2014.
[25] Xu S, Toth L, Schuman C, Lecomte J, Barnett M. Dislocation mediated variant selection for secondary twinning in compression of pure titanium. Acta Mater 2017;124:59–70.
[26] Guan D, Rainforth W, Ma L, Wynne B, Gao J. Twin recrystallization mechanisms and exceptional contribution to texture evolution during annealing in a magnesium alloy. Acta Mater 2017;126:132–44.

[27] Munroe N, Tan X, Gu H. Orientation dependence of slip and twinning in HCP metals. Scripta Mater 1997;36(12):1383–6.
[28] McCabe RJ, Kumar MA, Liu W, Tomé CN, Capolungo L. Revealing the effect of local stresses on twin growth mechanisms in titanium using synchrotron X-ray diffraction. Acta Mater 2021;221:117359.
[29] Christian JW, Mahajan S. Deformation twinning. Prog Mater Sci 1995;39(1-2):1–157.
[30] Zheng X, Zheng S, Wang J, Ma Y, Wang H, Zhou Y, et al. Twinning and sequential kinking in lamellar Ti-6Al-4V alloy. Acta Mater 2019;181:479–90.
[31] Jin S, Marthinsen K, Li Y. Formation of 11$\bar{2}$1 twin boundaries in titanium by kinking mechanism through accumulative dislocation slip. Acta Mater 2016;120:403–14.
[32] Li B, Ma E. Atomic shuffling dominated mechanism for deformation twinning in magnesium. Phys Rev Lett 2009;103:035503.
[33] Wang J, Yadav SK, Hirth JP, Tomé CN, Beyerlein IJ. Pure-shuffle nucleation of deformation twins in hexagonal-close-packed metals. Mater Res Lett 2013;1(3):126–32.
[34] Zhu KY, Vassel A, Brisset F, Lu K, Lu J. Nanostructure formation mechanism of α-titanium using SMAT. Acta Mater 2004;52(14):4101–10.
[35] Wen M, Liu G, Gu J-F, Guan W-M, Lu J. Dislocation evolution in titanium during surface severe plastic deformation. Appl Surf Sci 2009;255(12):6097–102.
[36] Wu S, Fan K, Jiang P, Chen S. Grain refinement of pure Ti during plastic deformation. Mater Sci Eng A 2010;527(26):6917–21.
[37] Wu X, Tao N, Hong Y, Xu B, Lu J, Lu K. Microstructure and evolution of mechanically-induced ultrafine grain in surface layer of AL-alloy subjected to USSP. Acta Mater 2002;50(8):2075–84.
[38] Vinogradov AY, Stolyarov VV, Hashimoto S, Valiev RZ. Cyclic behavior of ultrafine-grain titanium produced by severe plastic deformation. Mater Sci Eng A 2001;318(1-2):163–73.
[39] Sajadifar SV, Wegener T, Yapici GG, Niendorf T. Effect of grain size on the very high cycle fatigue behavior and notch sensitivity of titanium. Theor Appl Fract Mech 2019;104:102362.
[40] Fréour S, Gloaguen D, François M, Guillen R, Girard E, Bouillo J. Determination of the macroscopic elastic constants of a phase embedded in a multiphase polycrystal-application to the β-phase of a Ti-17 titanium based alloy. Mater Sci Forum 2002;404–407:723–8.
[41] Fréour S, Gloaguen D, François M, Perronnet A, Guillén R. Determination of single-crystal elasticity constants in a cubic phase within a multiphase alloy: X-ray diffraction measurements and inverse-scale transition modelling. Int J Appl Crystallogr 2005;38(1):30–7.
[42] Vinogradov A, Nagasaki S, Patlan V, Kitagawa K, Kawazoe M. Fatigue properties of 5056 Al-Mg alloy produced by equal-channel angular pressing. Nanostruct Mater 1999;11(7):925–34.
[43] Vinogradov A. Fatigue limit and crack growth in ultra-fine grain metals produced by severe plastic deformation. Int J Mater Sci 2007;42(5):1797–808.
[44] Zuo JH, Wang ZG, Han EH. Effect of microstructure on ultra-high cycle fatigue behavior of Ti-6Al-4V. Mater Sci Eng A 2008;473(1-2):147–52.
[45] Szczepanski CJ, Jha SK, Larsen JM, Jones JW. Microstructural influences on very-high-cycle fatigue-crack initiation in Ti-6246. Metall Mater Trans A 2008;39(12):2841–51.
[46] Pan X, Xu S, Qian G, Nikitin A, Shanyavskiy A, Palin-Luc T, et al. The mechanism of internal fatigue-crack initiation and early growth in a titanium alloy with lamellar and equiaxed microstructure. Mater Sci Eng A 2020;798:140110.
[47] Du L, Pan X, Qian G, Zheng L, Hong Y. Crack initiation mechanisms under two stress ratios up to very-high-cycle fatigue regime for a selective laser melted Ti-6Al-4V. Int J Fatigue 2021;149:106294.